

# Persistent Deformation in a Post-Collisional Stable Continental Region: Insights from 20 Years of cGPS in Romania

Alexandra Muntean<sup>1\*</sup>, Laura Petrescu<sup>1,2</sup>, Boudewijn Ambrosius<sup>3</sup>, Felix Borleanu<sup>1</sup>, Eduard Ilie Nastase<sup>1</sup>, Ioan Munteanu<sup>4,5</sup>

1. National Institute for Earth Physics, Magurele, 077125, Romania
2. Faculty of Physics, University of Bucharest, Magurele, 077125, Romania
3. Faculty of Aerospace Engineering, Delft University of Technology, Delft, 2629HS, The Netherlands
4. Faculty of Geology and Geophysics, University of Bucharest, Bucharest, 010041, Romania
5. Romanian Academy Institute for Geodynamics “Sabba Stefanescu”, Bucharest, 020032, Romania

*Correspondence to:* Alexandra Muntean ([muntean@infp.ro](mailto:muntean@infp.ro)), Laura Petrescu ([laura.petrescu@infp.ro](mailto:laura.petrescu@infp.ro)), Boudewijn Ambrosius ([bacambrosius@gmail.com](mailto:bacambrosius@gmail.com)).

**Abstract.** The Carpathian Region, located at the edge of the East European Platform, presents a unique tectonic setting where major deformation associated with subduction and collision appears to have ceased around 8 million years ago. Yet vertical movements and present-day seismicity continued afterward, suggesting ongoing crustal deformation and challenging our understanding of intraplate earthquakes and the processes driving these phenomena in an area considered a stable continental interior. In this study, we analyze over two decades of continuous GPS (cGPS) data from 143 permanent stations to estimate both horizontal and vertical crustal motions, constructing the most accurate model of crustal deformation in the region to date. The estimated velocity field indicates a southward drift of the South Carpathians and Moesia relative to Eurasia, with velocities ranging from 0.5 to 2 mm/yr. We detect a more complex pattern of vertical uplift and subsidence in the foredeep, challenging a previously held view that this region is solely subsiding. This pattern may reflect localized uplift in response to processes such as the Vrancea Slab break-off beneath the South-East Carpathians. Crustal scale active faults accommodate the observed differential motion, fragmenting the foreland. Furthermore, using a regularized horizontal velocity vector field, we estimate strain rate variations, maximum shear strain, and dilatation patterns across Romania, which closely align with observed crustal earthquake mechanisms. This agreement validates our results and indicates a significant influence of surface plate kinematics on the observed seismicity, in addition to the deep Vrancea Slab dynamics. Our findings provide fundamental insights into the causes of crustal deformation at the transition between active collision zones and stable continental platforms, enhancing our understanding of intraplate seismicity in regions traditionally considered tectonically stable.

**Keywords:** deformation, GPS, crustal motion, geology, tectonics

## 1. Introduction

A key tectonic question lies in understanding the nature of active deformation and frequent seismicity in regions situated at the transition between active subduction/collision systems and more stable continental interiors. The Carpathian Region in Romania marks such a transition between the active Africa-Eurasia subduction system to the south and the stable continental core of Eurasia: the East European Platform (Fig. 1). Although this area is not considered a traditionally active plate boundary, with most geological evidence suggesting that major deformation

38 associated with the collision ceased around 8 million years ago (Mațenco and Bertotti, 2000), it continues to  
39 experience frequent crustal and subcrustal seismicity. Active deformation and seismicity are observed along major  
40 faults and geological contacts (e.g., swarms near Tg. Jiu and Galați, Craiu et al., 2017; Radulian et al., 2023;  
41 Borleanu et al., 2024). Notably, the Vrancea Slab, a relic lithospheric plate sinking, retreating and stretching  
42 beneath the East Carpathians Bend Zone, may still be coupled with the overlying crust, as suggested by the  
43 thermochronological studies, which showed a significant amount of uplift, post 8 Ma, especially along the Western  
44 flank of Focsani Basin (Necea et al., 2005, 2013, 2021). This coupling could be driving long-term surface  
45 deformation (Ismail-Zadeh, 2012; Petrescu et al., 2021), contributing to ongoing seismicity (Radulian et al., 2019;  
46 Petrescu et al., 2025) and exhibiting the largest present-day strain concentration in continental Europe (Wenzel et  
47 al., 1999).

48 Measuring crustal motion is crucial for understanding ongoing deformation processes and seismic hazards in such  
49 a tectonically complex region. In this study, we estimate both horizontal and vertical motions using Global  
50 Positioning System (GPS) data from permanent stations that operated in Romania in the past 20 years. These  
51 measurements provide key information about how the region is deforming and how this relates to the observed  
52 seismicity. The data also shed light on the connection between surface deformation and subsurface dynamics,  
53 including the potential role of the sinking slab in driving seismic activity. Furthermore, the GPS data allows us to  
54 assess whether deformation is concentrated along major fault zones or more broadly distributed across the crust,  
55 offering a clearer picture of how past tectonic events continue to shape the region's seismic behavior.

56 The first vertical velocity maps of Romania, based on repeated leveling data from first- and second-order national  
57 network lines, were published by Cornea et al. 1978, 1979a 1979b. Following the major earthquake of March 4,  
58 1977 (M7.2), high-accuracy leveling measurements allowed for the development of a more refined vertical  
59 velocity map (Popescu and Dragoescu, 1987). Subsequent research extended these efforts to the broader Carpatho-  
60 Balkan region (Joo et al., 1987). Dinter and Schmitt (2001), after two years of GPS monitoring in Romania, found  
61 no significant deformation but recommended expanding the network and conducting repeated measurements at  
62 two-year intervals to capture crustal dynamics better. Van der Hoeven et al. (2005) later published results from  
63 annual GPS campaigns conducted between 1997 and 2004. However, velocity solutions derived from temporary  
64 GPS deployments were subject to influences such as equipment changes, monument removals, and antenna setup  
65 inconsistencies, as well as local effects like sediment compaction and site instability. Compared to the high  
66 precision of modern continuous GPS (cGPS) solutions, the historical campaign data exhibit 3 to 4 times higher  
67 uncertainty (van der Hoeven et al., 2005). These limitations highlight the need for continuous GPS measurements  
68 to better resolve crustal and mantle dynamics in geologically active regions.

## 69 **2. Tectonic setting**

70 The tectonic evolution of the Romanian region is essential for understanding present-day deformation and seismic  
71 activity. The Carpathian Mountains dominate the topography, but significant faulting and seismicity are pervasive  
72 in the South and Southeast Carpathians and the surrounding foreland (Petrescu et al., 2021), underlain by the  
73 Moesian Platform (MP), a thick lithospheric block with Precambrian-aged basement, shaped by multiple tectonic  
74 phases throughout the Paleozoic and Mesozoic times (Fig. 1). The Moesian Platform (MP) is bounded by the

75 Carpathians to the north and the Balkans to the south. It is largely covered by Neogene sediments and extends  
76 eastward to the Black Sea, where its uplifted basement is exposed in the Dobrogea region. The platform is  
77 transected by several crustal-scale faults, such as the Intra-Moesian Fault (IMF) and the Capidava-Ovidiu Fault  
78 (COF) (Fig. 1).

79 To the northeast, the MP transitions into the East European Platform (EEP), a thick and geologically stable  
80 continental core that forms part of the Eurasian Plate. The boundary between the two is marked by the North  
81 Dobrogea Orogen (NDO) (Hippolyte, 2002), a remnant of the Hercynian Orogeny (Seghedi et al., 1999), located  
82 between the Peceneaga-Camena Fault (PCF) and Sfântul Gheorghe Fault (SFG, Fig. 1). Part of this now partially  
83 eroded orogen is buried beneath Neogene foredeep sediments from the younger Carpathian collision, while to the  
84 east, it has undergone uplift.

85 Over the past 20 million years, the Adria Plate, a promontory of the African or Nubian plate, has continuously  
86 pushed other oceanic plates and microplates north and east, leading to their collision with the stable Eurasian  
87 terranes and driving the Alpine-Carpathian orogeny (Balla, 1986; Barrier et al. 2018), essentially shaping the  
88 present-day European continent (Schmidt et al., 2020). In Romania, these microplates have been obliquely thrust  
89 over the MP, forming the South Carpathians, and collided with the passive margin of the East European Platform,  
90 creating a series of thrust faults and thin-skinned sedimentary nappes that make up the East Carpathians  
91 (Sandulescu, 1984; Mañenco and Bertotti, 2000; Csontos and Vörös, 2004).

92 Beneath the Southeast Carpathians, where multiple tectonic units interact, the notorious Vrancea Slab, a  
93 lithospheric block that is plunging almost vertically into the mantle (Ren et al., 2012), stretching and generating  
94 frequent high-magnitude destructive earthquakes in Romania, both at intermediate depths and in the overlying  
95 crust (Radulian et al., 2019; Petrescu et al., 2021; Enescu et al., 2023). Observing the crustal motions above this  
96 sinking slab provides a unique opportunity to gain fundamental insights into crustal deformation in a triple-  
97 junction tectonic setting (Besutiu et al., 2017). Major collisional related shortening deformation in the Carpathians  
98 is thought to have ended around 8-11 Ma, based on the cessation of late Miocene thrusting (Mañenco et al., 2007  
99 and references therein), while fission-track analysis suggests the onset of exhumation (or uplift) at 4 Ma in the SE  
100 Carpathians and 12 Ma in the East and South Carpathians (Sanders et al., 1999; Cloetingh et al., 2006). Present-  
101 day GPS measurements provide key insights into how these long-term geological processes continue to shape  
102 ongoing crustal motion and deformation, particularly in the Vrancea Zone (Fig. 1), where active subduction and  
103 slab-related dynamics are still influencing surface motion. The crustal deformations observed today are also  
104 influenced by the relative motion of surrounding crustal blocks, complicating the understanding of the region's  
105 complex and dynamic geological behavior.

### 106 **3. Continuous GPS (cGPS) Networks in Romania**

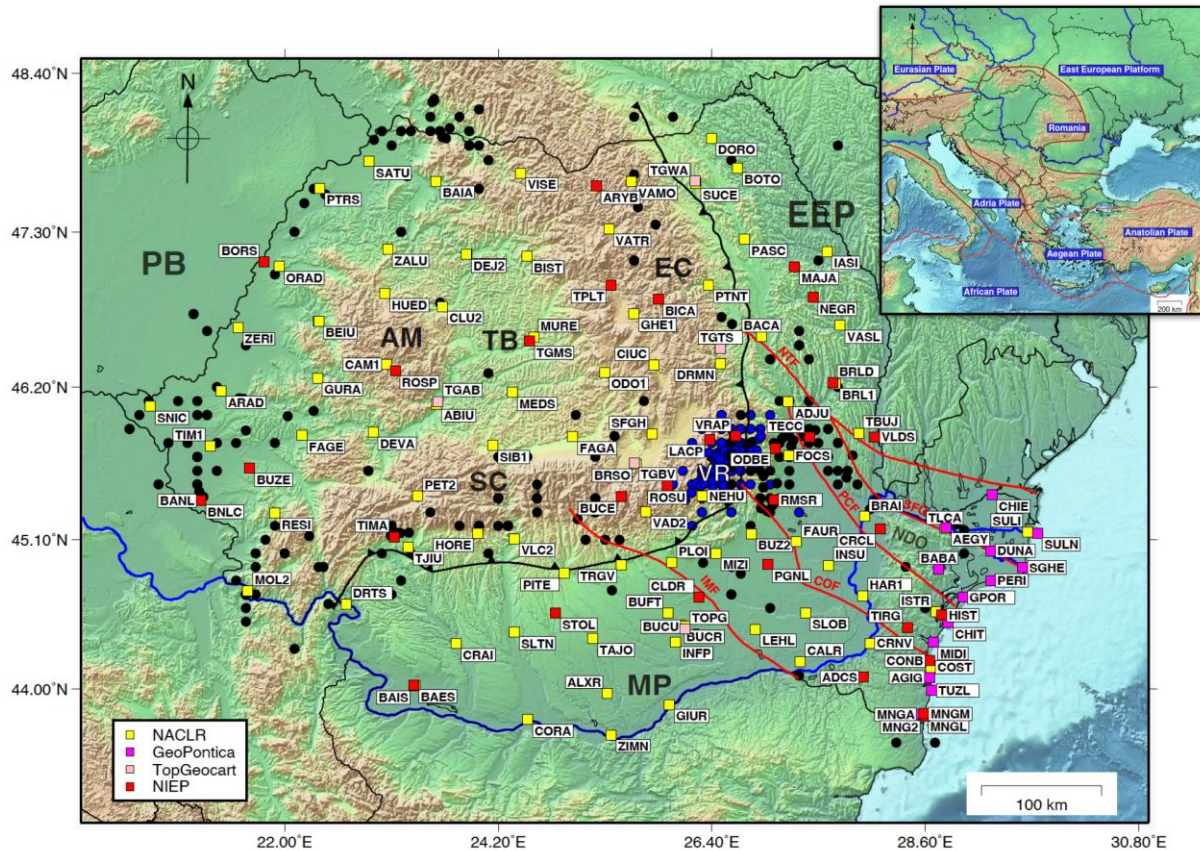
107 We analyzed data from cGPS stations across Romania, which are part of four different networks (Fig. 1). The  
108 primary network, supported by the National Institute for Earth Physics (NIEP), was first developed in 2001.  
109 Initially, the network consisted of seven stations, equipped with Leica CRS1000 receivers and LEIAT504 choke-  
110 ring antenna protected by a dome. These stations were placed in remote areas and were designed to operate with  
111 minimal maintenance, relying on power converters and batteries. Over time, the network has grown, and today it

112 includes 33 stations, with five of the original stations still in use. The newer stations are equipped with Leica  
113 GRX1200, LEIAR GR30, and GR50 receivers. Most of the antennas are Leica (LEIAT504, LEIAR10, LEIAR20)  
114 and are placed on concrete pillars. Only one is mounted on a polar mast (MNG2). The stations transmit real-time  
115 data via the internet, and NIEP is responsible for the equipment, installation, ongoing maintenance, and data  
116 analysis.

117 We also used GPS data from the GeoPontica network, developed by the National Research and Development  
118 Institute for Marine Geology and Geoecology (GeoEcoMar), the National Center for Monitoring and Alarm to  
119 Natural Marine Hazards – Euxinus, covering the period from 2013 to the present. This network includes 13  
120 stations, the antennas are mounted on a deep-drilled, braced monument. In addition, we included data from the  
121 ROMPOS (NACLR) network, managed by the National Agency for Cadastral and Land Registration, which  
122 consists of 86 reference stations across Romania. We were also granted access to data from the private TopGeocart  
123 network, which includes 8 stations. Most of these GPS antennas are mounted on building rooftops or fixed to the  
124 structures housing the receivers.

125 In total, this selection resulted in 143 available stations. The data are stored in a repository, organized by network,  
126 year and Julian day, in the Receiver Independent Exchange (RINEX) version 2 and 3 format, sampled at 30s  
127 intervals. For this study, we only selected stations that are (still) operational after January 01, 2024. This reduced  
128 the selection to 130 stations. Their locations and station acronyms are presented in Figure 1.

129  
130  
131  
132

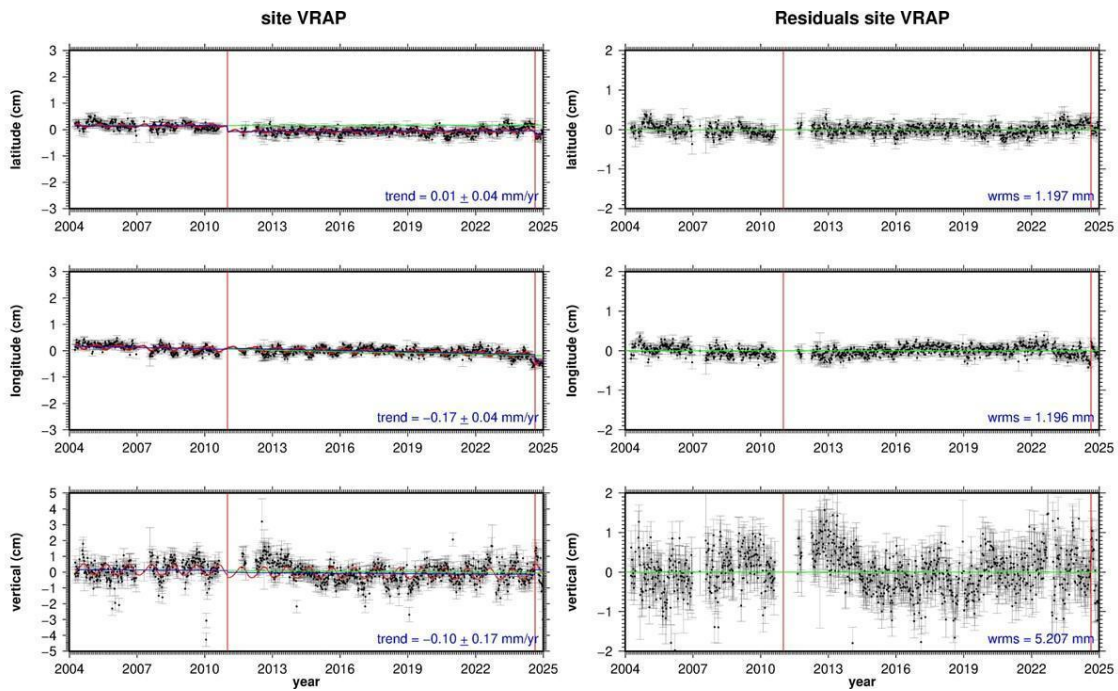


133  
 134 **Figure 1: The distribution of the available cGPS stations used in this study (coloured squares), and epicentres of**  
 135 **earthquakes with  $M_w > 3.5$  recorded in the Romanian earthquakes catalog (Romplus, Popa et al., 2022). Earthquakes**  
 136 **are color-coded by depth: black for crustal events ( $H < 60$  km), blue for intermediate-depth events. The major faults**  
 137 **are plotted as solid red lines and identified with their acronyms in a blue box: IMF - Intra-Moesian Fault, COF -**  
 138 **Capidava Ovidiu Fault, PCF - Peceneaga Camena Fault, NTF - New Trotuș Fault, and SFG - Sfântu Gheorghe Fault.**  
 139 **The old trust fault is represented by a solid, black, toothed line. The major tectonic units are in bold white characters:**  
 140 **AM - Apuseni Mountains, SC - South Carpathians, EC - East Carpathians, VR – Vrancea, NDO - North Dobrogea**  
 141 **Orogen, PB - Pannonian Basin, TB - Transylvanian Basin, EEP - East European Platform, and MP - Moesian Platform.**  
 142 **Further acronyms in the color legend box include: NACLR - National Agency for Cadastre and Land Registration,**  
 143 **GeoPontica - National Research-Development Institute for Marine Geology and Geocology GNSS network,**  
 144 **TopGeocart is a private company, operating its own GNSS network, NIEP - National Institute for Earth Physics. The**  
 145 **inset shows the regional tectonic setting, with plate boundaries indicated in red.**

#### 146 4. GPS data processing

147 For the data processing, we use the GipsyX software (Bertiger et al., 2020), developed at NASA’s Jet Propulsion  
 148 Laboratory (JPL), Pasadena, USA. It features Precise Point Positioning (PPP), which enables (daily) geodetic  
 149 position determination of a single GPS station. Accuracy can vary depending on the quality of the GPS receiver,  
 150 the antenna, and local conditions (e.g., multipath). Weekly updated data files, provided by JPL, contain precise  
 151 GPS satellite orbits, Earth Rotation Parameters (ERP), satellite clock corrections, spacecraft altitude information,  
 152 and so-called wide lane phase biases to enable signal ambiguity resolution. In addition, we apply ocean loading  
 153 corrections for each station, obtained from the Onsala Space Observatory, Chalmers University of Technology  
 154 (Bos and Scherneck, 2011). To model the wet tropospheric signal delays, we use data from VMF (Vienna Mapping  
 155 Functions) (re3data.org:VMF Data Server).

156 Processing the recordings from the 130 selected stations with this software resulted in a repository with daily  
 157 solutions for each station. Subsequently, to reduce noise, we combined the daily solutions into weekly ones. Then,  
 158 we converted the reference plate of these solutions to the Eurasian tectonic reference plate using the ITRF14  
 159 rotation parameters of that plate (Altamimi et al., 2017). From this data, we created a time series for each station.  
 160 Next, we estimated a linear trend (velocity) and yearly and half-yearly seasonal signals. In addition, for  
 161 undocumented changes, the estimation model also includes position jumps at times identified from an inspection  
 162 of the raw time series. All recent time series are affected by a reference frame change on August 19, 2024, by  
 163 JPL. These are now also modeled as position jumps. An example of the results is presented in Figure 2 for the  
 164 long-lived station VRAP. Apparently, this station was re-equipped in 2011, and from the vertical residuals, it  
 165 seems that it took a few years to settle down on its original monument.



166  
 167 **Figure 2: Time series of the VRAP station. The left panel shows the raw series with the modeled functions. The red**  
 168 **curve represents the estimated yearly and half-yearly functions. In the left panel the green line represents the estimated**  
 169 **velocity before the first jump. The vertical red lines represent position jumps. The right panel shows the residuals after**  
 170 **subtracting the modeled functions, including the estimated position jumps.**

#### 171 4.1 Horizontal time series selection and quality control

172 In this step, to ensure the best possible quality of the time series solutions, we selected stations with uncertainties  
 173 (sigmas) less than 0.2 mm/yr and velocity vectors smaller than 2 mm/yr. We consider that these criteria guarantee  
 174 a reliable selection of credible solutions. However, a small number of these sites still exhibit anomalous velocities.  
 175 These are likely caused by local effects such as landslides, station instability, local geological conditions,  
 176 subsurface compaction, undocumented antenna changes, and multipath interference. The main reason is that most  
 177 GPS antennas are mounted on buildings and unstable steel rods. In our analysis, we try to model them as position  
 178 jumps. The dates of these “unknown” jumps were established using a manual process by examining the “raw”  
 179 time series plots for each station.

180 This process automatically eliminates the shorter lived time series, reducing the number of accepted solutions to  
 181 99, with the shortest series extending more than four years. This means that all 99 accepted solutions satisfy the

182 criterion established by Blewitt et al. (2001), who claim that the series should be longer than two and a half years  
183 for a reliable estimate of the seasonal terms, which is vital for the reliability of the velocity estimate.

184 The accuracies ( $\sigma$ ) at the 95% confidence level were estimated using the weighted root mean square (WRMS) of  
185 the fit according to the formula:

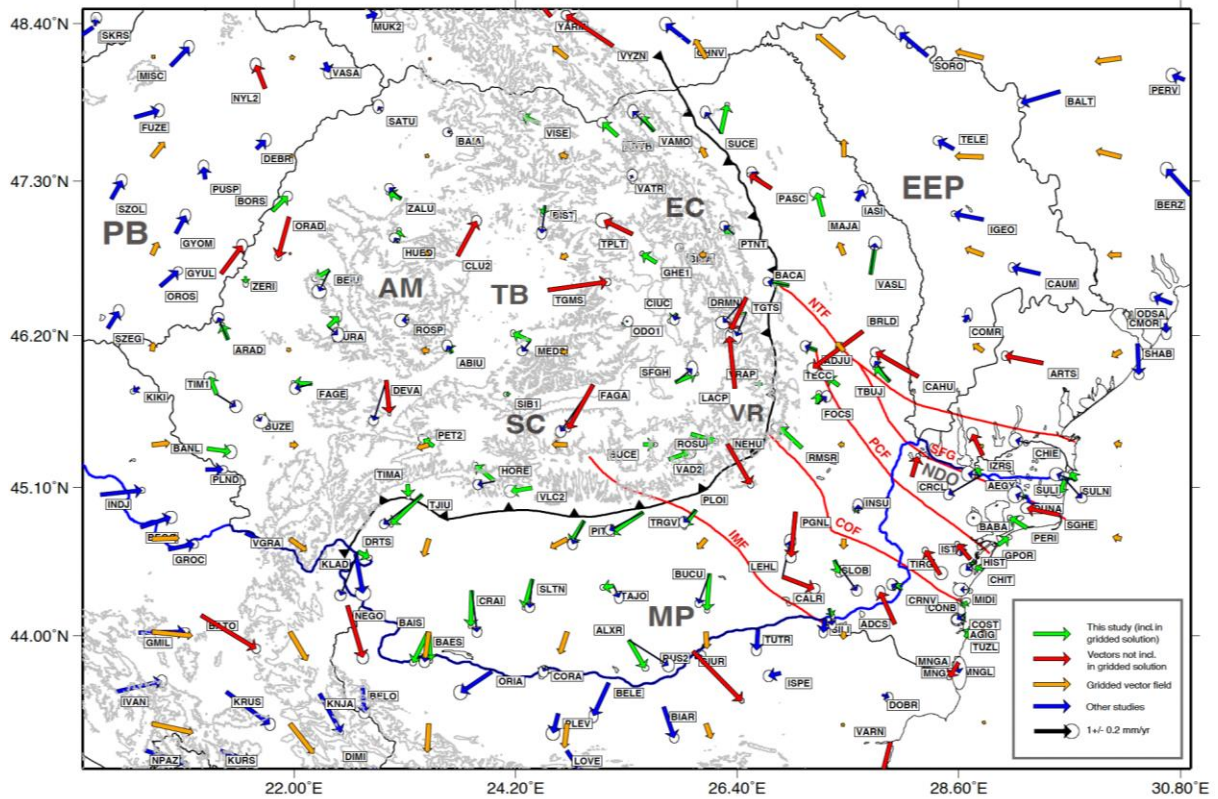
$$186 \quad \sigma = \frac{2 \cdot WRMS}{2.4 \cdot T_{span}}$$

187 where  $T_{span}$  is the length of the time series in years. This approach provides robust and realistic estimates of  
188 velocities and their uncertainties, and yields results comparable with those obtained using other commonly used  
189 algorithms, such as HECTOR and MIDAS. For some stations, our uncertainties are smaller than literature values,  
190 which is primarily due to the longer time series used in this study. We also compared our results with those of  
191 Piña-Valdés (2022) for stations with common solutions and found an average difference of less than 0.08 mm/yr.  
192 This level of agreement demonstrates general consistency, although earlier processing campaigns did not benefit  
193 from the reprocessing strategies and data quality controls applied here. The results for the 99 accepted sites are  
194 summarized in Table S1 of the Supplementary Material.

#### 195 **4.2 Creating a gridded, smooth horizontal velocity field**

196 To create a smooth, coherent representation of the computed time series solutions, we use a spatial gridding  
197 approach: we set up an 8 x 8 grid of latitude and longitude nodes with each node linked to a square search box.  
198 The size of these boxes depends on the distance (in km) between nearby nodes, ensuring the north-south and east-  
199 west dimensions are equal. We calculate the median of the absolute velocity vectors of the sites contained inside  
200 each search box. In the next step, we eliminate outliers with a velocity larger than two times the median. Then,  
201 we calculate the average of the EW and NS velocity components of the remaining solutions. During this process,  
202 22 of the 99 solutions are excluded as outliers. The final result is a gridded dataset of 47 nodes showing the  
203 velocities for each node. The other 17 nodes are not presented since there were no Romanian cGPS stations  
204 available in the search area (see Table S2, SM).

205 When we include the literature (Piña-Valdés et al., 2022; Serpelloni et al., 2022), solutions for the countries  
206 neighbouring Romania, the number of solutions increases to 160. After applying the aforementioned editing step,  
207 this number decreases to 133. These solutions are based on a collection of shorter time series from before 2021.  
208 Nevertheless, they provide valuable additional information.



209

210

211

212

213

**Figure 3: GPS-derived horizontal velocity vectors with respect to the ITRF-2014 Eurasian plate according to Altamimi et al. (2017). Green vectors represent our results, blue vectors were taken from Piña-Valdés et al. (2022) . The red vectors were excluded while creating the interpolated velocity field on a regular (8 x 8) grid, represented as orange vectors. The error ellipses are 95% confidence level. Faults and acronyms are as in Figure 1.**

214

### 4.3 Vertical data selection

215

216

217

218

219

220

221

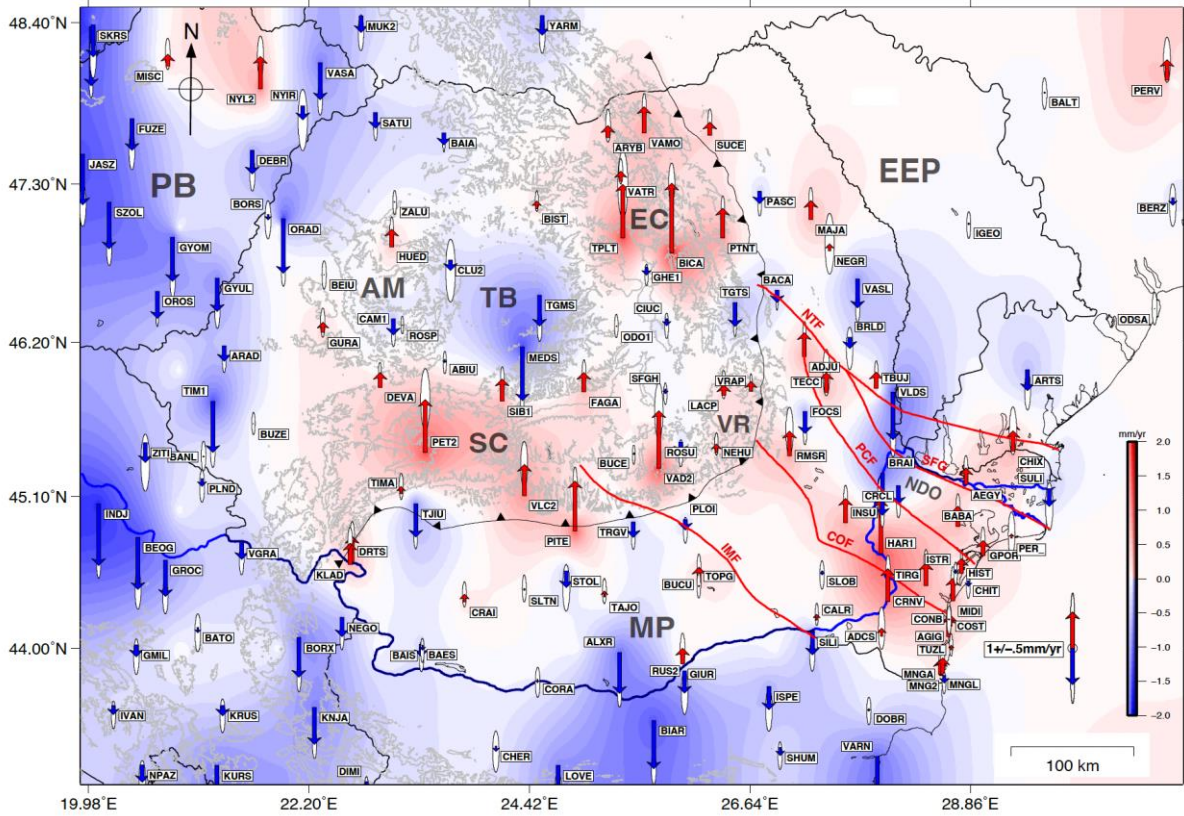
222

For the vertical component, we apply a different approach. This component is hardly affected by horizontal station instabilities, but mostly by undocumented antenna changes. We tackle this problem by estimating vertical position jumps at the dates when we see them appearing in the time series. Furthermore, we only select solutions with an absolute velocity of  $< 2$  mm/yr and an accuracy of  $< 1.0$  mm/yr, which we consider to be credible solutions. Some sites show larger subsidence, but these are mostly located in coastal areas, on slow landslides, and compacting sedimentary areas. As a result, from the 130 available solutions of the four Romanian permanent networks, 95 solutions were accepted (Fig. 4). The results are presented in Figure 4 and Table S3 (SM). We also compared our solutions with those of Piña-Valdés (2022), and found an average difference of less than 0.03 mm/yr.

223

224

When we include the literature solutions, the pattern does not change much. It mostly adds subsidence sites in the area west and south-west of Romania. The total number of accepted vertical sites increased to 145.



225  
 226 **Figure 4: GPS-derived vertical velocity vectors. Red vectors indicate uplift, while blue vectors indicate subsidence. The**  
 227 **background is a gridded interpolation field. The error ellipses are the 95% confidence level. Faults and acronyms are**  
 228 **as in Figure 1.**

229 **4.4 Strain rate estimation**

230 To better understand deformation and seismic hazard in this complex tectonic region, we further estimate strain  
 231 rate from the interpolated horizontal vector field of GPS velocities (Fig. 3). We use the open-source software  
 232 STRAINTOOL, which employs the VISR (Velocity Interpolation for Strain Rate) algorithm developed by Shen  
 233 et al. (2015). This algorithm interpolates our gridded solution to derive horizontal strain rates across the region,  
 234 using a weighted least squares approach on a more dense regular grid. At each grid point, the horizontal velocity  
 235 field is approximated by a bilinear function and a Gaussian function based on the distance between the  
 236 interpolation grid point and the other grid points is used for distance-weighting. This algorithm allows us to obtain  
 237 the spatial variation of strain rate, including the maximum shear strain rate (which indicates how much the crust  
 238 is laterally distorted), and the dilatational strain rate (which reflects areas of extension or compression). These  
 239 parameters are crucial for understanding the tectonic regime, whether a region is being compressed, extended, or  
 240 sheared, and how this deformation relates to observed earthquake focal mechanisms.

241 **5. Results**

242 **5.1 The horizontal velocity field**

243 Many horizontal velocity measurements indicate a predominantly southward movement in the MP, with variations  
 244 spanning approximately  $\pm 20$  degrees toward the southeast and southwest (Fig. 3). The IMF appears to mark a  
 245 slight orientation change from S-SE to S-SW oriented motion vectors. This shift is also reflected in the South

246 Carpathians, which are obliquely thrust over the MP, defined by strong and sometimes sharp lateral variation in  
247 rheology across the major faults like IMF or COF, which imposed the formation of tear-faults and oblique ramps  
248 into the Carpathian Orogen (Fig. 3). Hence, the magnitude and direction of motion vary significantly across the  
249 IMF and COF or other major faults in the MP and foreland units in general, like PCF and TF, that are defining  
250 crustal blocks with different rheologies, thermal history, and response under the orogenic loading. In contrast,  
251 vectors in the East European Platform (EEP) show a slight northwestward motion relative to the Eurasian plate.  
252 This shift occurs across the PCF and TF, which define the boundaries of the North-Dobrogea Orogen (Fig. 3), a  
253 transitional zone between the EEP margin and the MP. As a result, the EEP undergoes a subtle yet persistent  
254 movement relative to Eurasia, diverging from the southward-moving MP through a series of crustal-scale faults  
255 that accommodate lateral displacement.

256 The Transylvanian Basin (TB) and the East Carpathians, on the other hand, show minimal horizontal motion. GPS  
257 stations in these areas indicate limited deformation, with inconsistent directional patterns and low overall  
258 coherence in movement. Small horizontal motions are observed in the Pannonian Basin (PB) with an NNE  
259 direction, which gets reoriented close to the Apuseni Mountains in different directions (see Figs. 1 and 3).

260 Overall, the foreland region, particularly the MP, seems to be drifting southward, while the other areas remain  
261 relatively stable, indicating that the foreland is more dynamically active in comparison to the surrounding regions.

## 262 **5.2 The vertical velocity field**

263 The Carpathians predominantly experience significant uplift (Fig. 4), concentrated in the East Carpathians (e.g.,  
264 BICA, TPLT), and the South Carpathians (e.g., VAD2, and PITE). While some scattered stations (ROSU, TGTS)  
265 indicate subsidence, the overall trend suggests uplift rates ranging between 0.5 and 2 mm/yr. The Vrancea bend  
266 zone is an interesting exception because it only shows a minor uplift (e.g., LACP and VRAP).

267 The foreland region exhibits an intricate interplay of uplift and subsidence. The Moesian Platform (MP), which  
268 occupies the area bounded by the Carpathians, the Balkans and the Black Sea, shows a north-south dichotomy in  
269 vertical motion. In its southern part, across the E-W trending Danube river and towards the Balkans, the crust is  
270 predominantly subsiding. Northward and northeastward toward the Carpathians, the Capidava-Ovidiu Fault, the  
271 trend gradually transitions to uplift. The most pronounced uplift occurs in Dobrogea, the exposed basement of the  
272 Moesian Platform near the Black Sea, where all geodetic stations record consistent uplift along the coast and the  
273 Danube. Notably, the Danube changes its course northward across this transition zone.

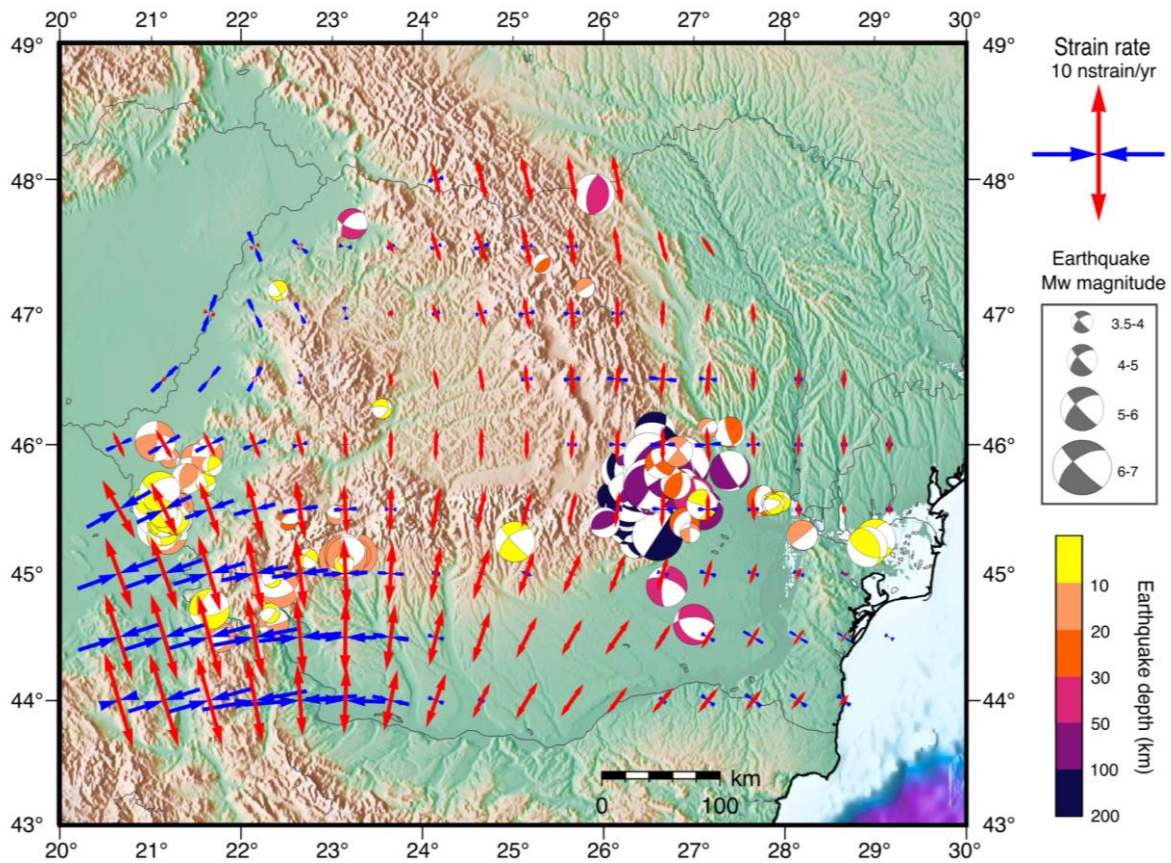
274 The East European Platform (EEP), forming the eastern foreland of the Carpathians, exhibits only minor vertical  
275 movements. Several stations in its northern part record slight uplift, which transitions southward into subsidence  
276 toward the Troțuș Fault. This subsiding trend extends farther south into parts of the North Dobrogea Orogen  
277 (NDO), continuing across the SFG and the PCF, which delineates the boundary with the Moesian Platform (MP).  
278 On the opposite side, the MP is undergoing uplift, reflecting strong differential crustal deformation along these  
279 seismically active fault networks.

280 In the backarc region relative to the Carpathians, in the Transylvanian and Pannonian basins, estimated crustal  
281 motions suggest subsidence relative to stable Eurasia. However, the Apuseni Mountains, a prominent highland  
282 dividing the two subsiding basins, exhibit a cluster of stable and slightly uplifted motion vectors. Plotted vectors

283 range between -2 and +2 mm/yr, with an uncertainty of 1.0 mm/yr (Table S3 of the SM). This is a general feature  
284 for most stations in Europe.

### 285 5.3 GPS-estimated strain rates

286 Figure 5 shows the estimated strain rate variation across Romania, from the regularized horizontal velocity vector  
287 field, while Figs. 6a and b show the distribution of maximum shear strain rate and dilatation. The dilatation rate  
288 quantifies the extent to which the Earth's crust is either expanding or contracting. It is derived by combining the  
289 principal strain rates, with positive values indicating extension and negative values indicating contraction. High  
290 positive dilatation values are indicative of regions experiencing extension, while negative values suggest  
291 compression, as seen in processes like thrust faulting. On the other hand, the maximum shear strain rate measures  
292 the degree of shear deformation within the crust, without affecting its overall volume. This is determined by  
293 calculating the difference between the principal strain rates. Elevated shear strain rates are associated with regions  
294 undergoing significant shear deformation, such as strike-slip fault zones, while lower values typically occur in  
295 areas experiencing predominantly extensional or compressional deformation.

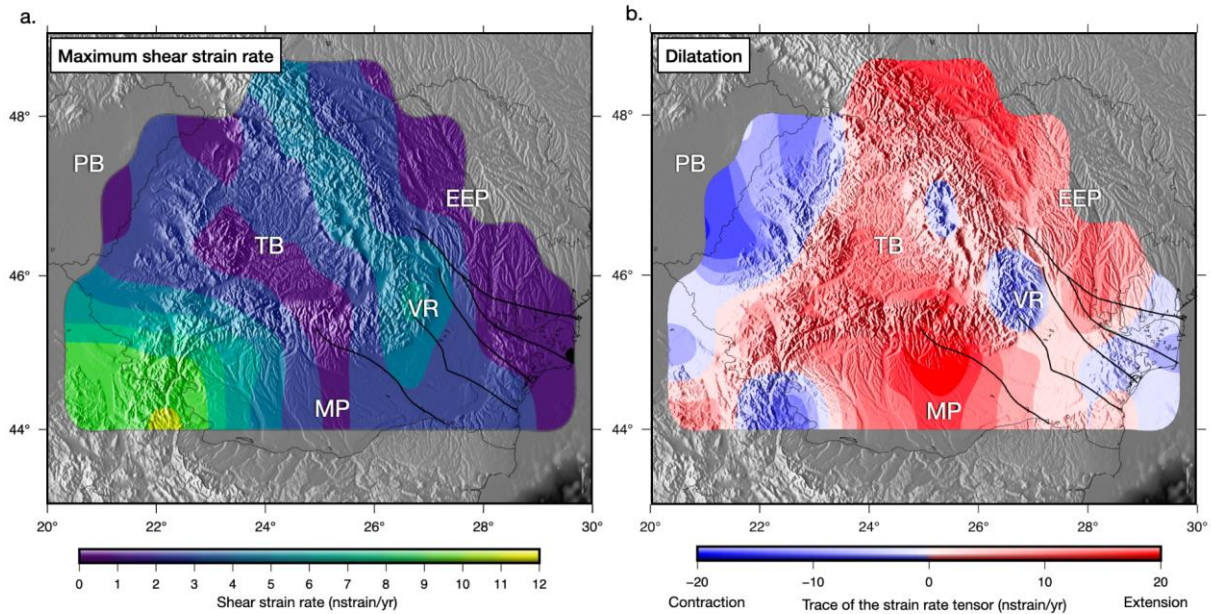


296  
297 **Figure 5: Map showing the principal axes of strain rates determined from the regularized GPS horizontal**  
298 **velocity vector field from this study and mechanisms of earthquakes with  $M_w > 3.5$  from the REFMC**  
299 **catalogue (Radulian et al., 2019).**

300 The distribution of strain rates is quite complex (Fig. 5 and Table S4, SM), which is expected given the region's  
301 complicated tectonic framework, with multiple blocks of diverse strengths converging to form a sinuous orogenic

302 track. The highest strain rates were estimated in the southwest, at the border between Romania and Serbia. This  
303 region also experiences the highest shear strain rate (Fig. 6a).

304 Dilatation patterns estimated from the strain tensor show a transition from compression in the PB to extension in  
305 the intra-orogenic TB. The South Carpathians and the surrounding foreland regions, including the MP and the  
306 EEP, are predominantly characterized by extension (Fig. 6b). However, localized areas of compression are  
307 observed in the Eastern and South-East Carpathians, particularly in the Vrancea Zone.

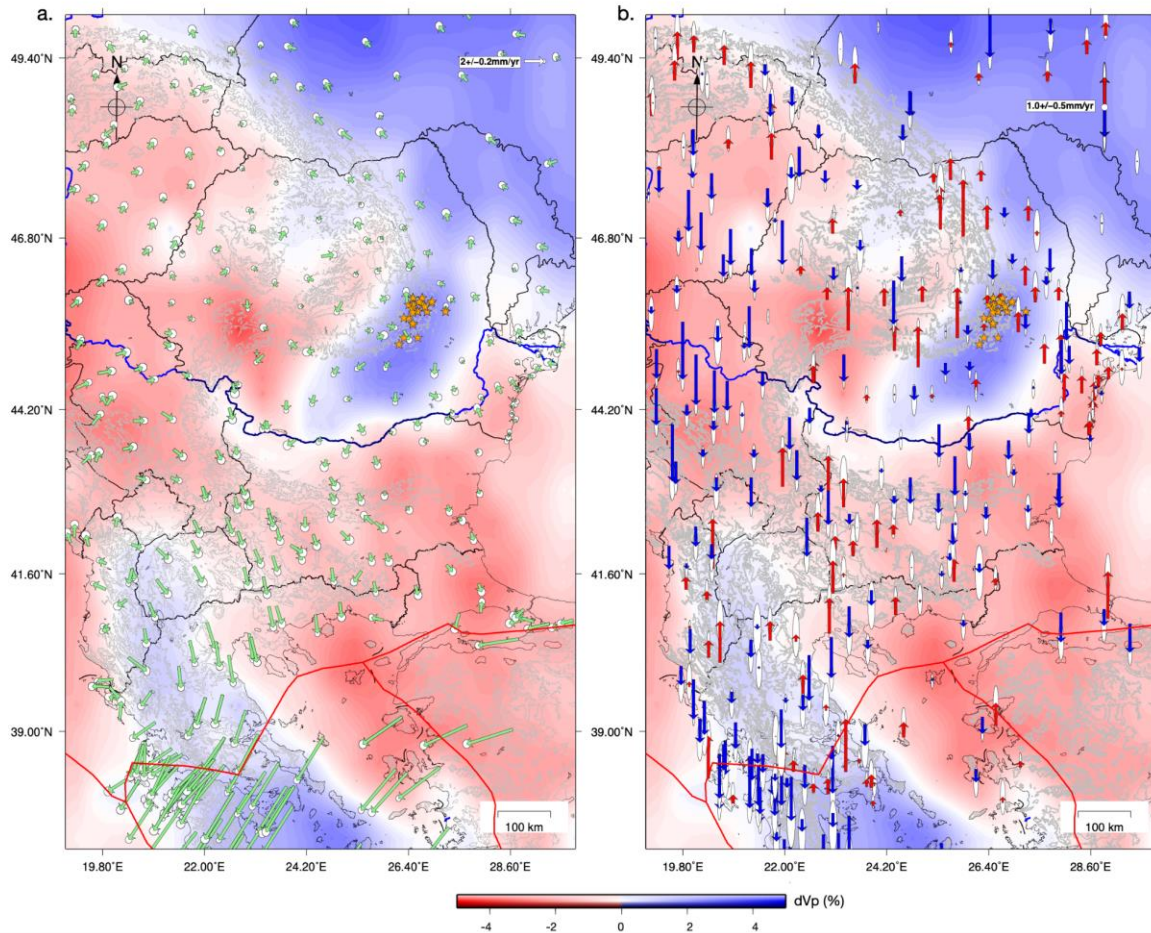


308  
309 **Figure 6: Maps showing (a) maximum shear strain rate and (b) dilatational strain rate (both in**  
310 **nanostrain/year), derived from the regularized GPS velocity field in Romania (Table S2, SM). The**  
311 **maximum shear strain rate illustrates the intensity and direction of lateral crustal deformation, while the**  
312 **dilatational strain rate is the trace of the strain rate tensor (volumetric rate of change) and indicates regions**  
313 **of extension (red-positive) and compression (blue-negative). Major faults are shown as thick black lines.**  
314 **Acronyms are described in the caption of Figure 1.**

## 315 6. Discussion

### 316 6.1 Regional tectonic context

317 To put our results in a broader context, we plot them against previous GPS-derived velocity vectors (Serpeloni et  
318 al., 2022; Piña-Valdés et al., 2022) in Fig. 7. While there is some overlap with the Romanian networks, the  
319 differences between datasets are minor. To reduce clutter in the figures and minimize the impact of large tectonic  
320 motions in the south, we excluded stations with an absolute horizontal velocity exceeding 7 mm/yr, as shown in  
321 Fig. 7a, horizontal and 7b, vertical, with the UU-07 seismic tomography model of Amaru et al. (2007), updated  
322 based on Wortel and Spakman (2000), at 200 km depth, serving as background.



323  
 324 **Figure 7: Regional horizontal (a) and vertical crustal motions (b) from this study, Serpeloni et al. (2022), and Piña-**  
 325 **Valdés et al. (2022). The horizontal vector field was scaled for visibility. The background colours show Vp seismic**  
 326 **velocity anomalies at 200 km depth from the UU-P07 seismic model of Amaru et al. (2007). Red lines mark the active**  
 327 **plate boundaries between Eurasia, Anatolia, and Aegean plates in the south. Orange stars mark earthquakes Mw > 6**  
 328 **from the Vrancea Zone (Radulian et al., 2019).**

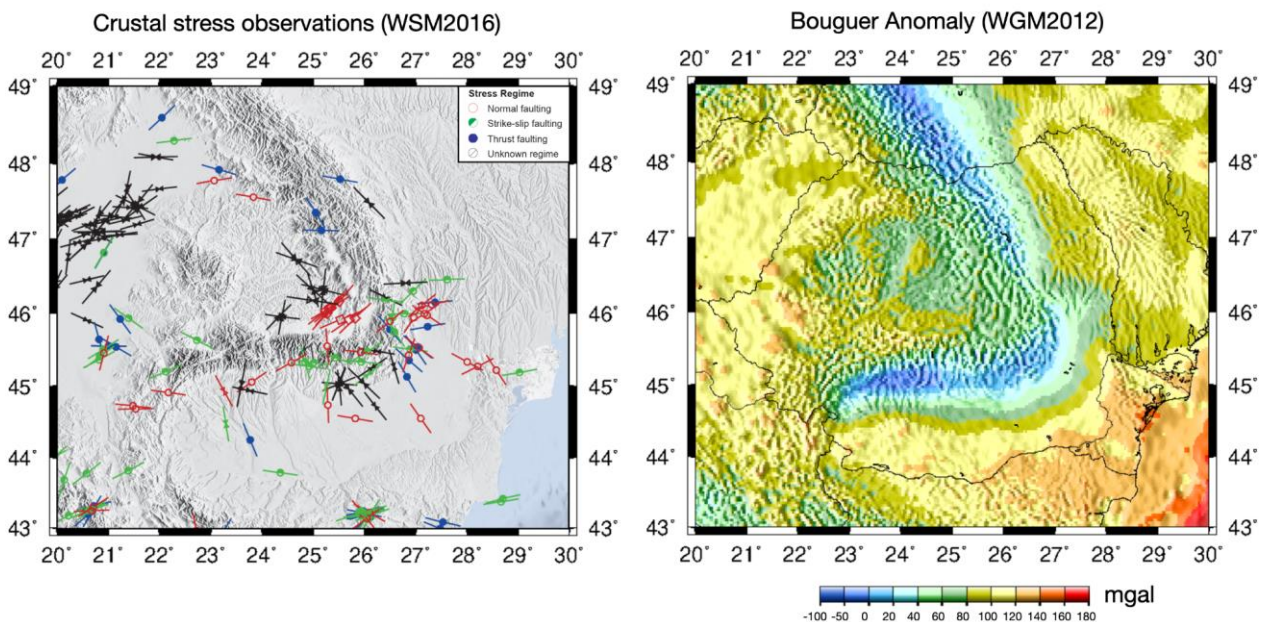
329 In the regional plate tectonic context, the observed velocity field highlights the complex interactions between  
 330 major tectonic plates and blocks that converged in this complex region. Seismic tomography shows the high  
 331 velocity thick cratonic lithosphere to the north-east, which is supposed to be tectonically stable, the Vrancea Slab  
 332 as an elongated high velocity block sinking beneath the Carpathians, and the Adria and the Hellenic slabs  
 333 subducting beneath the Balkan Peninsula (Fig. 7). To the south, crustal motion velocities increase significantly  
 334 (Fig. 7), reflecting the rapid motion of the Hellenic subduction system as the African Plate subducts beneath the  
 335 Eurasian Plate, driving southeastward deformation in Greece. Eastward, the Anatolian Plate is moving westward  
 336 due to tectonic escape caused by the northward collision of the Arabian Plate with Eurasia. This westward motion  
 337 is a dominant feature of the eastern Mediterranean and plays a key role in accommodating the overall regional  
 338 deformation.

339 To the west, the Pannonian Basin, a hyper-extended lithosphere back-arc basin, shows relatively low horizontal  
 340 deformation rates, suggesting it is currently tectonically stable, with mirror positive inversion of its eastern margin.  
 341 However, the influence of the Adriatic Plate, a promontory of the African Plate, is significant. The Adria Plate,  
 342 subducting eastwards (Fig. 7), exerts a northeastward push on the Carpathian-Pannonian system, contributing to  
 343 compressional forces and tectonic inversion along the basin (Bada et al, 2007). These larger-scale processes

344 interact with the local tectonic architecture, such as the Vrancea Slab and associated seismicity (orange stars in  
345 Fig. 7), resulting in a complex and heterogeneous deformation regime that bridges the stable cratonic lithosphere  
346 and the active subduction-driven tectonics to the south and south-west.

## 347 6.2 Correlation with fault systems and seismicity

348 Most seismically active crustal-scale faults and geological boundaries in Romania are located in the South and  
349 South-East Carpathians, as well as the foreland domains, which are crossed by several major faults (Fig. 1). While  
350 the Vrancea Slab is well known for generating subcrustal earthquakes with a dominant reverse faulting mechanism  
351 in an overall compressive regime, the crust above exhibits much more diverse deformation (Fig. 5) and stress  
352 patterns (Fig. 8), likely driven by a combination of surface plate kinematics and Vrancea Slab dynamics. Stress  
353 inversion of earthquake clusters in the crust (Petrescu et al., 2021) and geological indicators of stress from the  
354 World Stress Map (WSM2016, Heidbach et al., 2007) reveal a complex pattern of stress in the region (Fig. 8).



355 **Figure 8: Left: Crustal stress observations compiled from focal mechanisms, borehole breakouts, and other geological**  
356 **indicators, from the World Stress Map (Heidbach et al., 2018). Colours indicate the most likely stress regime. Right:**  
357 **Bouguer gravity anomalies from the World Gravity Map (WGM2012) maintained by the Bureau Gravimétrique**  
358 **International (Bonvalot et al., 2012).**

359 Although the GPS-derived strain rate field appears smooth at the regional scale, it consistently shows N-S  
360 extension throughout most of the study area and localized E-W compression in the southwestern corner (Fig. 6).  
361 This pattern reflects the long-wavelength deformation pattern resolved by the GPS velocity field, whereas the  
362 earthquake focal mechanisms capture the shorter-wavelength, fault-controlled deformation that accommodates  
363 this regional strain.

364 A localized cluster of thrust faulting stress regime indicators in the SE Carpathians broadly aligns with the negative  
365 dilatation rate derived from GPS vectors, suggesting localized compression at the bend zone (Fig. 6). This  
366 compressive region transitions into a mix of strike-slip and dominantly normal-faulting regimes (Fig. 8), aligning  
367 with our estimated dilatation rates that suggest an extensional regime throughout the foreland and the Carpathians  
368 (Fig. 6). This extension is supported by numerous normal fault earthquake swarms occurring near the SFG (Fig.

369 5 and Craiu et al., 2017). The South Carpathians have also recently experienced an intense seismic swarm of  
370 normal-faulting earthquakes in the South Carpathians (Radulian et al., 2023; Borleanu et al., 2024).

371 At the same time, the variability of focal mechanisms, especially among smaller-magnitude events (Mw 3-4),  
372 reflects the activation of secondary and oblique faults that accommodate local adjustments between the main  
373 regional stress regimes. Even within the overall extensional setting, these structures produce local pockets of  
374 compression or shear along inherited structures, consistent with a distributed deformation field. The compressive  
375 strain patch observed in the Eastern Carpathians (Fig. 6b) coincides with a cluster of thrust-faulting stress regime  
376 indicators (Fig. 8), supporting the reliability of the GPS-derived strain inversion and illustrating how localized  
377 compression and extension coexist within the same regional stress framework.

378 In the Moesian Platform, vertical movements are not uniform, but are accommodated differentially across crustal-  
379 scale fault systems. This variability likely arises from the differing rheological properties of crustal blocks that  
380 make up the MP (Mațenco et al., 2003; Petrescu et al., 2019) and the influence of pre-existing lithospheric  
381 heterogeneities (e.g., Bertotti et al., 2003; Tărăpoancă et al., 2004). As a result, many fault mechanisms in the MP  
382 exhibit both oblique and strike-slip components, producing seemingly chaotic fault patterns (Fig. 5). Focal  
383 mechanism solutions in these regions may show greater variability, particularly in areas of pronounced strain  
384 partitioning, such as near large-offset faults or shear zones.

### 385 **6.3 Interactions between slab dynamics and surface uplift**

386 Our results indicate a clear uplift trend in the foredeep basin area, supporting a typical post-collisional rebound  
387 and uplift behavior, as observed in many other orogenic systems. These observations contrast with previous  
388 models (van der Hoeven et al., 2005; Merten et al., 2005, 2010), which suggest that subsidence dominated the  
389 evolution of the region as a typical response to slab subduction and retreat (Tărăpoancă et al., 2004). This  
390 represents a notable change from earlier interpretations, which tended to highlight uplift in the Dobrogea forebulge  
391 while assuming subsidence further towards the Carpathian Orogen. This is also in line with some historical long-  
392 term repeated leveling methods (e.g., Popescu and Lazarescu, 1987; Joo, 1987) and is further supported by recent  
393 InSAR analyses (Poncos et al., 2022). While the continued uplift in Dobrogea is confirmed, the GPS data suggest  
394 that this uplift extends into the foredeep, highlighting the presence of vertical motions in the foredeep basin that  
395 are not solely driven by active subduction dynamics.

396 The discrepancy may reflect either a shift in the tectonic regime over time or methodological limitations in  
397 capturing ongoing geodynamic processes. The observed uplift may be associated with a partial decoupling  
398 between the subducting lower lithosphere and the overlying crust (Petrescu et al., 2021), allowing stress relaxation  
399 and isostatic rebound of the upper crust in the foreland. This scenario is consistent with the distribution of  
400 intermediate-depth seismicity and the focal mechanism patterns observed in Vrancea. In addition, Mitrofan et al.  
401 (2014) suggested a partial transmission of deformation from the slab to the crust, further supporting the idea of  
402 vertical stress transfer from the mantle to the surface.

403 While the continued uplift in Dobrogea is confirmed, the GPS data suggest that this uplift extends into the  
404 foredeep, highlighting the presence of vertical motions in the foredeep basin that are not solely driven by active  
405 subduction dynamics. Instead, the observed uplift in both regions may be linked to slab break-off, a late-stage

406 process in the subduction and continental collision cycle (Andrews and Billen, 2009). As mentioned before, the  
407 Dobrogea uplifting area at the transition to the Black Sea Basin is parallel with the SE Carpathians, suggesting  
408 again the interplay between collisional processes affecting the Orogen and flexural response of the lower plate  
409 with the forebulge outward (from the orogen) migration with coeval uplift and erosion.

410 Seismic imaging suggests that the Vrancea Slab has partially torn and rotated at ~150 km depth (Martin et al.,  
411 2006), leaving a deeper slab segment (200-310 km) still weakly attached (Heidbach et al., 2007). If break-off  
412 continues to be active (Müller et al., 2010), asthenospheric upwelling through the torn slab segment (Petrescu et  
413 al., 2023) may be dynamically supporting present-day uplift in both the SE Carpathians and foredeep. Numerical  
414 simulations of subduction-collision systems with spontaneous slab break-off (Duretz et al., 2011) predict post-  
415 break-off uplift rates of 0.1-0.8 km/Myr (0.1-0.8 mm/yr), which closely match our observed uplift. Additionally,  
416 an increase in slab dip may promote low-wavelength lithospheric folding following continental collision (e.g.,  
417 Cloetingh et al., 2004; Mařenco et al., 2007), contributing further to the uplift observed in both the SE Carpathians  
418 and the foredeep.

419 Our results also reveal a significant uplift in the East Carpathians (Fig. 4), not just the SE Carpathians, raising the  
420 question of whether past slab break-off there (Nemcok et al. 1998) could still be influencing present-day vertical  
421 motions. Geodynamic reconstructions suggest that the subducted passive margin of the East European Platform  
422 progressively broke off from north to south along the East Carpathians (Sperner et al., 1996), culminating in the  
423 currently detaching Vrancea Slab (Sperner et al., 2001; Koulakov et al., 2010; Lorincz and Houseman, 2010).  
424 While the initial isostatic response to slab break-off is expected to occur within a few million years (Duretz et al.,  
425 2011) or up to 7 million years after convergence stops (Andrews and Billen, 2009), prolonged effects such as  
426 mantle flow, residual buoyancy, and lower-crustal flow could be sustaining regional uplift. This interpretation is  
427 further supported by Bouguer gravity anomalies (Fig. 8), which show relatively positive values (0–40 mGal) over  
428 the mountain belt, suggesting the presence of denser material at depth or incomplete isostatic compensation. The  
429 north-to-south younging of post-collisional volcanism (Seghedi et al., 2004) suggests that slab detachment  
430 propagated southward over time, with the East Carpathians experiencing earlier break-off than the SE Carpathians.  
431 If asthenospheric upwelling and lithospheric weakening were significant during that time, they could have led to  
432 prolonged crustal adjustments that continue to manifest as uplift today.

433 In addition to the SE and East Carpathians, we also identify localized uplift in the South Carpathians. This region  
434 marks the collision between the Dacia Block and the Moesian Platform, where oblique thrusting over the thick  
435 Moesian lithosphere (Mařenco et al., 1997) may be inducing flexural or isostatic responses (Bertotti et al., 2003).  
436 Bouguer gravity anomalies in this area transition from strongly negative values (~-100 mGal) near the foredeep  
437 in the south to over +100 mGal at the contact with the Transylvanian Basin (Fig. 8), indicating a shift from thick,  
438 low-density crust to denser material in the north. This pattern suggests differential isostatic compensation, where  
439 northward crustal thinning leads to less mass deficit and reduced buoyancy, potentially causing flexural uplift.  
440 This contrast could drive vertical displacements, as observed. Alternatively, deeper mantle processes, such as  
441 residual slab dynamics or lithospheric-scale deformation associated with orogenic curvature, may also influence  
442 the observed uplift.

443

## 444 **7. Conclusions**

445 This study integrates the most stable and longest GPS data records over a period of 20 years in the Carpathian  
446 region in Romania. Our results mark a significant improvement in spatial coverage and resolution of vertical and  
447 horizontal crustal motions in a tectonically complex region sitting at the transition between dynamically active  
448 subduction systems and the stable East European Platform, with additional influences exerted by a descending  
449 slab.

450 We observe significant horizontal southward motion in the Moesian Platform, minimal motion in the  
451 Transylvanian Basin and East Carpathians, and a slight north-west motion of the Eastern European Platform, in a  
452 Eurasian reference frame. The relative motions between these regions generate a dominantly extensional strain  
453 field with localized zones of compression and shear, broadly consistent with stress regimes inverted from  
454 earthquake clusters, although individual events capture more localized deformation heterogeneity.

455 Earlier studies in the region relied on campaign-style GPS observations. In contrast, our dataset includes cGPS  
456 data from 130 stations spanning more than 20 years, providing improved spatial density and temporal resolution.  
457 Our extended and more reliable data also reveal uplift in the foredeep of the SE Carpathians, challenging a  
458 previously held view that this area is solely subsiding based on temporary GPS station data. This insight provides  
459 a fresh perspective on the region's slab dynamics, which may be influenced by slab break-off and the fragmented  
460 nature of the foreland, with its blocks of varying rheological strength. These differential vertical motions are  
461 accommodated by seismically active faults on a crustal scale.

462 Overall, this study significantly advances our understanding of the tectonic processes that shape regions at the  
463 intersection of active subduction/collision zones and stable continental platforms. It provides fundamental  
464 constraints on the interplay between slab dynamics, surface plate kinematics, and the resulting crustal  
465 deformation, an essential step toward improving seismic hazard assessment.

### 466 **Code availability**

467 The GipsyX software is licensed to the Department of Geophysics of the University of Bucharest (UNIBUC). We  
468 were allowed to use this software in an ongoing collaboration with UNIBUC. The strain rate estimation code  
469 STRAINTOOL (Anastasiou et al., 2021) is available at <https://github.com/DSOlab/StrainTool> (accessed in  
470 January 2025). Most figures were made using the open-source GMT software (Wessel et al., 2013).

### 471 **Data availability**

472 The RINEX-format GNSS data (sampled at 30s intervals) analysed in this study are only available from the NIEP  
473 (National Institute of Earth Physics) network online at <http://gps.infp.ro/#/>. The rest of the data can be made  
474 available from the organisations responsible with their maintenance upon reasonable request and data sharing  
475 agreements. All individual velocity solutions and strain rate estimates from this study are provided in the  
476 Supplementary Material.

477

478 **Author contributions**

479 **AM:** Conceptualization, Methodology, Data Curation, Formal analysis, Investigation, Writing - Original Draft,  
480 Visualization **LP:** Formal analysis, Writing - Original Draft, Visualization **BA:** Software, Data Curation, Formal  
481 analysis, Visualization, Writing - Review & Editing, Supervision **FB:** Writing - Review & Editing **EN:** Writing -  
482 Review & Editing, Installation and Stations Maintenance **IM:** Writing - Review & Editing

483 **Competing interests**

484 The authors declare that they have no conflict of interest.

485 **Acknowledgments**

486 We acknowledge the Netherlands Research Centre for Integrated Solid Earth Science (ISES) for the initial  
487 establishment in 2001 of seven cGPS stations in Romania dedicated to long term geodetic and geophysical  
488 research in the region. This early enterprise comprised a collaborative effort of the University of Bucharest (V.  
489 Mocanu), the National Institute for Earth Physics (L. Munteanu), the Delft University of Technology (B.A.C.  
490 Ambrosius) and the Utrecht University (W. Spakman). We thank the National Research and Development Institute  
491 for Marine Geology and Geo-Ecology, National Center for Monitoring and Alarm to Natural Marine Hazards –  
492 Euxinus, as well as the National Agency for Cadaster and Land Registration, and the TopGeocart company for  
493 providing access to their data.

494 **Financial support**

495 This research was carried out within the NUCLEU project, SOL4RISC Program which is supported by the  
496 Ministry of Education and Research, project nr. PN23360201. This work was also supported by the European  
497 Union (Next Generation EU instrument) through the National Recovery and Resilience Plan, "PNRR-III-C9-2022  
498 – I5 Establishment and operationalization of Competence CentersBertiger" competition, "Competence Center for  
499 Climate Change Digital Twin for Earth forecasts and societal redressment: DTEClimate" project, contract  
500 no.760008/30.12.2022, code 7/16.11.2022.

501 **References**

502 Altamimi, Z., Métivier, L., Rebischung, P., Rouby, H., and Collilieux, X.: ITRF2014 plate motion model, *Geophys. J. Int.*,  
503 209, 1906–1912, <https://doi.org/10.1093/gji/ggx136>, 2017.

504 Anastasiou D.G., Papanikolaou X., Ganas A., and Paradissis D.: StrainTool: A software package to estimate strain tensor  
505 parameters. Zenodo; Version 1.1, <https://doi.org/10.5281/zenodo.5501234>, 2021.

506 Amaru, M. L.: Global travel time tomography with 3-D reference models, PhD thesis, Utrecht Univ., Utrecht, Netherlands,  
507 2007.

508 Andrews, E. R. and Billen, M. I.: Rheologic controls on the dynamics of slab detachment, *Tectonophysics*, 464, 60-69,  
509 <https://doi.org/10.1016/j.tecto.2007.09.004>, 2009.

510 Bada, G., Horváth, F., Dövényi, P., Szafián, P., Windhoffer, G. and Cloetingh, S.: Present-day stress field and tectonic  
511 inversion in the Pannonian basin, *Global Planet. Change*, 58, 165-180, <https://doi.org/10.1016/j.gloplacha.2007.01.007>, 2007.

- 512 Balla, Z.: Palaeotectonic reconstruction of the central Alpine-Mediterranean belt for the Neogene, *Tectonophysics*, 127, 213-  
513 243, [https://doi.org/10.1016/0040-1951\(86\)90062-4](https://doi.org/10.1016/0040-1951(86)90062-4), 1986.
- 514 Bertiger, W., Bar-Sever, Y., Dorsey, A., Haines, B., Harvey, N., Hemberger, D., Heflin, M., Lu, W., Miller, M., Moore, A.W.,  
515 Murphy, D., Ries, P., Romans, L., Sibois, A., Sibthorpe, A., Szilagyi, B., Vallisneri, M., and Willis, P.: GipsyX/RTGx, a new  
516 tool set for space geodetic operations and research, *Advances in Space Research*, 66, 469–489,  
517 <https://doi.org/10.1016/j.asr.2020.04.015>, 2020.
- 518 Bertotti, G., Maţenco, L. and Cloetingh, S. A. P. L.: Vertical movements in and around the south-east Carpathian foredeep:  
519 lithospheric memory and stress field control. *Terra Nova*, 15, 299-305, 2003.
- 520 Beşuţiu, L., Manea, V., Pomeran, M.: Vrancea seismic zone as an unstable triple junction: new evidence from observations  
521 and numerical modelling. In: 9th Congress of the Balkan Geophys. Soc, vol. 2017. European Association of Geoscientists &  
522 Engineers, 1-5, 2017 <https://doi.org/10.3997/2214-4609.201702541>
- 523 Blewitt, G., Lavallée, D., Clarke, P., and Nurutdinov, K.: A new global mode of Earth deformation: Seasonal cycle detected,  
524 *Science*, 294, 2.342-2.345, <https://doi/10.1126/science.106532001>, 2001.
- 525 Bonvalot, S., Balmino, G., Briais, A., M. Kuhn, Peyrefitte, A., Vales, Biancale, R., Gabalda, G., Moreaux, G., Reinquin, F.,  
526 and Sarrailh, M.: World Gravity Map, 1:50000000 map, Eds.: BGI-CGMW-CNES-IRD, Paris, 2012.
- 527 Bos. M. S., and Scherneck, H., G.: Ocean tide loading provider, <http://holt.oso.chalmers.se/loading/index.html>, 2011.
- 528 Borleanu F., Petrescu L., Fojtikova L., Munteanu I., Silvennoinen H., Placinta A.O., Oros E., and Enescu B.: ML 5.7 Southern  
529 Carpathians earthquake sequence: Insights from seismic observations, ESC2024-S17/50-808,  
530 [https://www.erasmus.gr/UsersFiles/microsite1277/Documents/ESC2024\\_Abstract\\_Book.pdf](https://www.erasmus.gr/UsersFiles/microsite1277/Documents/ESC2024_Abstract_Book.pdf), 2024.
- 531 Cloetingh, S. A. P. L., Burov, E., Matenco, L., Toussaint, G., Bertotti, G., Andriessen, P. A. M., Wortel, M. J. R. and Spakman,  
532 W.: Thermo-mechanical controls on the mode of continental collision in the SE Carpathians (Romania), *Earth Planet. Sc. Lett.*,  
533 218, 57-76, 2004.
- 534 Cloetingh, S., Bada, G., Maţenco, L., Lankreijer, A., Horváth, F. and Dinu, C.: Modes of basin (de) formation, lithospheric  
535 strength and vertical motions in the Pannonian-Carpathian system: inferences from thermo-mechanical modelling, *Geo. Soc.*  
536 *Mem.*, 32, 207-221, DOI: 10.1144/GSL.MEM.2006.032.01.12, 2006.
- 537 Cornea, I., Dragoescu, I., Popescu, M. N., and Visarion, M.: Monography of recent vertical crustal movements in the S. R. of  
538 Romania (in Romanian), Preprint Central Inst. of Phys., 100, 1978.
- 539 Cornea, I., and Popescu, M. N.: The Vrancea Earthquake of March 4. 1977 and the Recent crustal vertical movements in  
540 Romania. In Cornea & Radu (Editors): Seismological Research of March 4. 1977 Earthquake (in Romanian), Preprint Central  
541 Inst. of Phys., 559 - 568, 1979a.
- 542 Cornea, I., Dragoescu, I., Popescu, M. N., and Visarion, M.: Map of recent vertical crustal movements of the territory of S. R.  
543 of Romania (in Romanian), *St. Cerc. Geol., Geofiz., Geogr., Geofizica*, 17, 3-20, 1979b.
- 544 Craiu, A., Craiu, M., Diaconescu, M. and Marmureanu, A.: 2013 Seismic swarm recorded in Galati area, Romania: focal  
545 mechanism solutions, *Acta Geod. Geophys.*, 52, 53-67, 2017.
- 546 Csontos, L., and Vörös, A.: Mesozoic plate tectonic reconstruction of the Carpathian region, *Palaeogeography,*  
547 *Palaeoclimatology, Palaeoecology*, 210, 1-56, <https://doi.org/10.1016/j.palaeo.2004.02.033>, 2004.
- 548 Dinter, G., and Schmitt, G.: Three Dimensional Plate Kinematics in Romania, *Nat. Hazards*, 23, 389–406,  
549 <https://doi.org/10.1023/A:1011116615142>, 2001.
- 550 Duretz, T., Gerya, T. V. and May, D. A.: Numerical modelling of spontaneous slab breakoff and subsequent topographic  
551 response, *Tectonophysics*, 502, 244-256, <https://doi.org/10.1016/j.tecto.2010.05.024>, 2011.
- 552 Enescu, B., Ghita, C., Moldovan, I.A. and Radulian, M.: Revisiting Vrancea (Romania) intermediate-depth seismicity: some  
553 statistical characteristics and seismic quiescence testing. *Geosciences*, 13, 21, <https://doi.org/10.3390/geosciences13070219>,  
554 2023.
- 555 Heidbach, O., Ledermann, P., Kurfeß, D., Peters, G., Buchmann, T., Matenco, L., Negut, M., Sperner, B., Müller, B., and  
556 Nuckelt, A.: Attached or not attached: slab dynamics beneath Vrancea, Romania, In: International symposium on strong  
557 Vrancea earthquakes and risk mitigation, 4–20, 2007.
- 558 Heidbach, O., Rajabi, M., Cui, X., Fuchs, K., Müller, B., Reinecker, J., Reiter, K., Tingay, M., Wenzel, F., Xie, F. and Ziegler,  
559 M.O.: The World Stress Map database release 2016: Crustal stress pattern across scales. *Tectonophysics*, 744, 484-498, 2018.
- 560 Hippolyte, J.C.: Geodynamics of Dobrogea (Romania): new constraints on the evolution of the Tornquist–Teisseyre Line, the  
561 Black Sea and the Carpathians, *Tectonophysics*, 357, 33-53, [https://doi/10.1016/S0040-1951\(02\)00361-X](https://doi/10.1016/S0040-1951(02)00361-X), 2002.

- 562 Ismail-Zadeh, A., Maţenco, L., Radulian, M., Cloetingh, S. and Panza, G.: Geodynamics and intermediate-depth seismicity in  
563 Vrancea (the south-eastern Carpathians): current state-of-the art. *Tectonophysics*, 530, 50-79, DOI:  
564 10.1016/j.tecto.2012.01.016, 2012.
- 565 Joó, I., Arabadžijski, D., Fűry, M., Meščerski, I. N., Mihăila, M., Mladenovski, M. M., Németh, Z., Steinberg, J., Thury, J.,  
566 Vanko, J., and Wyrzykowski, T.: New investigations or recent vertical movements in the Carpatho-Balkan region, *J.*  
567 *Geodyn.*, 8, 99-113, [https://doi.org/10.1016/0264-3707\(87\)90028-7](https://doi.org/10.1016/0264-3707(87)90028-7), 1987.
- 568 Koulakov, I., Zaharia, B., Enescu, B., Radulian, M., Popa, M., Parolai, S. and Zschau, J.: Delamination or slab detachment  
569 beneath Vrancea? New arguments from local earthquake tomography, *Geochem. Geophys. Geosy.*, 11,  
570 <https://doi.org/10.1029/2009GC002811>, 2010.
- 571 Krézsek, C., Lăpădat, A., Maţenco, L., Arnberger, K., Barbu, V., and Olaru, R.: Strain partitioning at orogenic contacts during  
572 rotation, strike-slip and oblique convergence: Paleogene-Early Miocene evolution of the contact between the South  
573 Carpathians and Moesia, *Global Planet. Change*, 103, 63–81, <https://doi.org/10.1016/j.gloplacha.2012.11.009>, 2013.
- 574 Lorinczi, P., and Houseman, G.: Lithospheric gravitational instability beneath the Southeast Carpathians, *Tectonophysics*, 474,  
575 322–336, <https://doi.org/10.1016/j.tecto.2008.05.024>, 2009.
- 576 Maţenco L, Zoetemeijer R, Cloetingh S, and Dinu C.: Lateral variations in mechanical properties of the Romanian external  
577 Carpathians: inferences of flexure and gravity modelling. *Tectonophysics*, 282,147-166, 1997.
- 578 Maţenco, L., and Bertotti, G.: Tertiary tectonic evolution of the external East Carpathians (Romania), *Tectonophysics*, 316,  
579 255–286, [https://doi.org/10.1016/S0040-1951\(99\)00261-9](https://doi.org/10.1016/S0040-1951(99)00261-9), 2000.
- 580 Maţenco L, Bertotti G, Cloetingh S, and Dinu C; Subsidence analysis and tectonic evolution of the external Carpathian-  
581 Moesian platform region during Neogene times. *Sed Geol*, 156(14), 71-94, 2003.
- 582 Maţenco, L., Bertotti, G., Leever, K., Cloetingh, S.A.P.L., Schmid, S.M., Tărăpoancă, M., and Dinu, C.: Large-scale  
583 deformation in a locked collisional boundary: Interplay between subsidence and uplift, intraplate stress, and inherited  
584 lithospheric structure in the late stage of the SE Carpathians evolution, *Tectonics*, 26, <https://doi.org/10.1029/2006TC001951>,  
585 2007.
- 586 Merten, S., Andriessen, P. A. M., Juez-Larré, J., Bertotti, G. V., and Dunai, T. J.: Dating the exhumation of the Romanian  
587 Carpathians: first results from apatite (U-Th)/He thermochronology, *Abstract from Geophysical Research Abstracts*, 7, 08138,  
588 <https://meetings.copernicus.org/www.cosis.net/abstracts/EGU05/08138/EGU05-J-08138.pdf>, 2005.
- 589 Merten S., Matenco L., Foeken J. P. T., Stuart F. M., and Andriessen P. A. M.: From nappe stacking to out-of-sequence  
590 postcollisional deformations: Cretaceous to Quaternary exhumation history of the SE Carpathians assessed by low-temperature  
591 thermochronology, *Tectonics*, 29, <https://doi.org/10.1029/2009TC002550>, 2010.
- 592 Müller, B., Heidbach, O., Negut, M., Sperner, B. and Buchmann, T.: Attached or not attached—evidence from crustal stress  
593 observations for a weak coupling of the Vrancea slab in Romania, *Tectonophysics*, 482, 139-149,  
594 <https://doi.org/10.1016/j.tecto.2009.08.022>, 2010.
- 595 Necea, D., Fielitz, W., and Matenco, L.: Late Pliocene–Quaternary tectonics in the frontal part of the SE Carpathians: Insights  
596 from tectonic geomorphology, *Tectonophysics*, 410, 137-156, <https://doi.org/101016/j.tecto.2005.05.047>, 2005.
- 597 Necea D., Fielitz W., Kadereit A., P.A.M. Andriessen P.A.M., and Dinu C.: Middle Pleistocene to Holocene fluvial terrace  
598 development and uplift-driven valley incision in the SE Carpathians, Romania, *Tectonophysics*, 602, 332-354,  
599 <https://doi.org/10.1016/j.tecto.2013.02.039>, 2013.
- 600 Necea, D., Juez-Larré, J., Matenco, L., Andriessen, P. A.M., and Dinu C.: Foreland migration of orogenic exhumation  
601 during nappe stacking: Inferences from a high-resolution thermochronological profile over the Southeast Carpathians, *Global*  
602 *Planet. Change*, 200, 103457, <https://doi.org/10.1016/j.gloplacha.2021.103457>, 2021.
- 603 Nemcok, M., Pospisil, L., Lexa, J., and Donelick, R.A.: Tertiary subduction and slab break-off model of the Carpathian–  
604 Pannonian region, *Tectonophysics*, 295, 307-340, [https://doi.org/10.1016/S0040-1951\(98\)00092-4](https://doi.org/10.1016/S0040-1951(98)00092-4), 1998.
- 605 Petrescu, L., Stuart, G., Tataru, D., and Grecu, B.: Crustal structure of the Carpathian Orogen in Romania from receiver  
606 functions and ambient noise tomography: how craton collision, subduction and detachment affect the crust. *Geophys. J. Int.*,  
607 218, 163-178, <https://doi.org/10.1093/gji/ggz140>, 2019.
- 608 Petrescu, L., Borleanu, F., Radulian, M., Ismail-Zadeh, A., and Maţenco, L.: Tectonic regimes and stress patterns in the  
609 Vrancea Seismic Zone: Insights into intermediate-depth earthquake nests in locked collisional settings, *Tectonophysics*, 799,  
610 228688, <https://doi.org/10.1016/j.tecto.2020.228688>, 2021.
- 611 Petrescu, L., Mihai, A. and Borleanu, F.: Slab tear and rotation imaged with core-refracted shear wave anisotropy., *J. Geodyn.*,  
612 157, 101985, <https://doi.org/10.1016/j.jog.2023.101985>, 2023.

- 613 Petrescu, L. and Enescu, B.: Seismicity of a relic slab: space–time cluster analysis in the Vrancea Seismic Zone. *Earth, Planets*  
614 *and Space*, 77, 6., <https://doi.org/10.1186/s40623-025-02136-6>, 2025.
- 615 Piña-Valdés, J., Socquet, A., Beauval, C., Doin, M.-P., D’Agostino, N., and Shen, Z.-K.: 3D GNSS velocity field sheds light  
616 on the deformation mechanisms in Europe: Effects of the vertical crustal motion on the distribution of seismicity, *J. Geophys.*  
617 *Res.-Sol. Ea.*, 127, e2021JB023451, <https://doi.org/10.1029/2021JB023451>, 2022.
- 618 Poncos, V., Stanciu, I., Teleaga, D., Maţenco, L., Bozsó, I., Szakács, A., Birtas, D., Toma, S.A., Stanica, A., and Radulescu,  
619 V.: An Integrated Platform for Ground-Motion Mapping, Local to Regional Scale; Examples from SE Europe. *Remote*  
620 *Sensing*, 14, 1046, [10.3390/rs14041046](https://doi.org/10.3390/rs14041046), 2022.
- 621 Popa, M., Chircea, A., Dinescu, R., Neagoe, C., Grecu, B., and Borleanu, F.: Romanian earthquake catalogue  
622 (ROMPLUS). *Mendeley Data*, 2, 2022.
- 623 Popescu, M. N., and Drăgoescu, I.: Maps of recent vertical crustal movements in Romania: Similarities and differences, *J.*  
624 *Geodyn.*, 8, 123-136, [https://doi.org/10.1016/0264-3707\(87\)90030-5](https://doi.org/10.1016/0264-3707(87)90030-5), 1987.
- 625 Radulian, M., Bălă, A., Ardeleanu, L., Toma-Dănilă, D., Petrescu, L., and Popescu, E.: Revised catalogue of earthquake  
626 mechanisms for the events occurred in Romania until the end of twentieth century: REFMC, *Acta Geod. Geophys.*, 54, 3-18,  
627 <https://doi.org/10.1007/s40328-018-0243-y>, 2019.
- 628 Radulian, M., Popa, M., Dinescu, R., and Bala, A.: Location improvements for the twin crustal earthquakes recorded in  
629 February 2023 in Gorj County, Romania. *International Multidisciplinary Scientific GeoConference: SGEM*, 23(1.1), 57-64,  
630 2023.
- 631 Ren, Y., Stuart, G., Houseman, G., Dando, B., Ionescu, C., Hegedüs, E., Radovanović, S., and Shen, Y.: Upper mantle  
632 structures beneath the Carpathian–Pannonian region: Implications for the geodynamics of continental collision, *Earth Planet.*  
633 *Sc. Lett.*, 349, 139–152. <https://doi.org/10.1016/j.epsl.2012.06.037>, 2012.
- 634 re3data.org: VMF Data Server; editing status 2024-05-15; re3data.org - Registry of Research Data Repositories,  
635 <https://doi.org/10.17616/R3RD2H>
- 636 Sanders, C., Andriessen, P., and Cloetingh, S.: Life cycle of the East Carpathian orogen: erosion history of a doubly vergent  
637 critical wedge assessed by fission track thermochronology, *J. Geophys. Res.*, 104, 29095–29112,  
638 <https://doi.org/10.1029/1998JB900046>, 1999.
- 639 Schmid, S.M., Fügenschuh, B., Kounov, A., Maţenco, L., Nievergelt, P., Oberhänsli, R., Pleuger, J., Schefer, S., Schuster, R.,  
640 Tomljenović, B., and Ustaszewski, K.: Tectonic units of the Alpine collision zone between Eastern Alps and western Turkey,  
641 *Gondwana Res.*, 78, 308-374, <https://doi.org/10.1016/j.gr.2019.07.005>, 2020.
- 642 Seghedi, A., Lang, B. and Heimann, A.: The deformational history of North Dobrogean Hercynian basement as reflected in  
643 new <sup>39</sup>Ar/<sup>40</sup>Ar determinations, *Romanian Journal of Tectonics and Regional Geology*, 77, 64-65,  
644 <https://doi.org/10.3906/YER-1101-20>, 1999.
- 645 Seghedi, I., Downes, H., Vaselli, O., Szakács, A., Balogh, K. and Pécskay, Z.: Post-collisional Tertiary–Quaternary mafic  
646 alkalic magmatism in the Carpathian–Pannonian region: a review, *Tectonophysics*, 393, 43-62,  
647 <https://doi.org/10.1016/j.tecto.2004.07.051>, 2004.
- 648 Serpelloni, E., Cavaliere, A., Martelli, L., Pintori, F., Anderlini, L., Borghi, A., Randazzo, D., Bruni, S., Devoti, R., Perfetti,  
649 P., and Cacciaguerra, S.: Surface Velocities and Strain-Rates in the Euro-Mediterranean Region From Massive GPS Data  
650 Processing, *Front. Earth Sci.*, 10, 907897, <https://doi.org/10.3389/feart.2022.907897>, 2022.
- 651 Shen, Z. K., Wang, M., Zeng, Y., and Wang, F.: Strain determination using spatially discrete geodetic data, *Bull. Seismol.*  
652 *Soc. Am.*, 105, 2117-2127, <https://doi.org/10.1785/0120140247>, 2015.
- 653 Sperner, B.: Computer programs for the kinematic analysis of brittle deformation structures and the Tertiary tectonic evolution  
654 of the Western Carpathians. *Tübingen Geoscientific Works (TGA) Series A. Geology, Paleontology, Stratigraphy* 27  
655 (NEBIS)001536648EBI01, 1996.
- 656 Sperner, B., Lorenz, F., Bonjer, K., Hettel, S., Müller, B., and Wenzel, F.: Slab break-off–abrupt cut or gradual detachment?  
657 New insights from the Vrancea Region (SE Carpathians, Romania), *Terra Nova*, 13, 172-179, <https://doi.org/10.1046/j.1365-3121.2001.00335.x>, 2001.
- 659 Tărăpoancă, M., Garcia-Castellanos, D., Bertotti, G., Matenco, L., Cloetingh, S., and Dinu, C.: Role of the 3-D distributions  
660 of load and lithospheric strength in orogenic arcs: polystage subsidence in the Carpathians foredeep, *Earth Planet. Sc. Lett.*,  
661 221, 163–180, [https://doi.org/10.1016/S0012-821X\(04\)00068-8](https://doi.org/10.1016/S0012-821X(04)00068-8), 2004.
- 662 Van der Hoeven, A., Mocanu, V., Spakman, W., Nutto, M., Nuckelt, A., Matenco, L., Munteanu, L., Marcu, C., and  
663 Ambrosius, B.: Observation of present-day tectonic motions in the Southeastern Carpathians: Results of the ISES/CRC-461  
664 GPS measurements, *Earth Planet. Sc. Lett.*, 239, 177-184, <https://doi.org/10.1016/j.epsl.2005.09.018>, 2005.

- 665 Wenzel, F., Lorenz, F., Sperner, B., and Oncescu, M. C.: Seismotectonics of the Romanian Vrancea area, Vrancea Earthquakes:  
666 Tectonics, Hazard and Risk Mitigation, 15–26, Kluwer Acad., 1999.
- 667 Wessel, P., W. H. Smith, R. Scharroo, J. Luis, and F. Wobbe: Generic Mapping Tools: Improved Version Released, Eos,  
668 Trans. AGU, 94, 409–410, <https://doi.org/10.1002/2013EO450001>, 2013.
- 669 Wortel, M.J.R. and Spakman, W.: Subduction and slab detachment in the Mediterranean-Carpathian region, Science, 290,  
670 1910-1917, <https://doi.org/10.1126/science290.5498.1910>, 2000.